JCST

Vol.34 No.6 Nov. 2019

ISSN 1000-9000(Print)
/1860-4749(Online)
CODEN JCTEEM

Journal of Computer Science & Technology

COMPUTER

SPONSORED BY INSTITUTE OF COMPUTING TECHNOLOGY
THE CHINESE ACADEMY OF SCIENCES &

CHINA COMPUTER FEDERATION

SUPPORTED BY NSFC

CO-PUBLISHED BY SCIENCE PRESS &

SPRINGER

Zhang MH, Yu JH, Zhang K *et al.* Artistic augmentation of photographs with droplets. JOURNAL OF COMPUTER SCIENCE AND TECHNOLOGY 34(6): 1294–1306 Nov. 2019. DOI 10.1007/s11390-019-1976-y

Artistic Augmentation of Photographs with Droplets

Mo-Han Zhang[1], Jin-Hui Yu[1,2], Kang Zhang[3,4], and Jun-Song Zhang[5]

[1] *State Key Laboratory of CAD & CG, Zhejiang University, Hangzhou 310027, China*

[2] *Department of Computer Science, Harbin Finance University, Harbin 150030, China*

[3] *Department of Computer Science, The University of Texas at Dallas, Richardson, TX 75080-3021, U.S.A.*

[4] *Faculty of Information Technology, Macau University of Science and Technology, Macau 999078, China*

[5] *National Engineering Research Center for E-Learning, Central China Normal University, Wuhan 430079, China*

E-mail: zhangmohan@zju.edu.cn; jhyu@cad.zju.edu.cn; kzhang@utdallas.edu; jszhang@outlook.com

Received April 9, 2019; revised August 29, 2019.

Abstract Artistic augmentation of photographs with water droplets aims at generating aesthetic yet realistic images, and thus differs from traditional augmented reality in two aspects. One difference lies in the adoption of a new image as the environment map in order to render reflected or refracted effects on the surface of inserted water droplets. The other difference is in modeling of water droplets including hanging droplets and resting droplets. These differences raise two research challenges: 1) how to adjust the brightness and colors of the new environment map to maintain visual consistency between the new environment map and the original input image; 2) how to model hanging and resting droplets aesthetically. This paper proposes a framework that addresses these two challenges and demonstrates the effectiveness of our framework by generating example augmented images.

Keywords artistic augmentation, augmented reality, illumination estimation, droplet modeling, image-based modeling

1 Introduction

Nature photography is usually taken outdoors and puts a stronger emphasis on the aesthetic value of photos than other photography genres. In nature photography, water droplets (droplets for short) resting on objects such as flowers and leaves or hanging from objects such as tree branches make photos look vivid, alive, and vibrant, as shown in Fig.1, where droplets glitter like jewels under the sunlight. The droplets reflect the sky and their surroundings, and thus enhance the photo's aesthetics and naturalness. However, capturing the sparkle and shimmer droplets resting on objects is not easy in an outdoor environment, because such visual effects depend heavily on the weather (after the rain for instance), appropriate lighting and camera angle.

(a) (b)

Fig.1. Droplets (a) resting on objects or (b) hanging from objects.

On the other hand, numerous photographs have been taken with excellent lighting and composition, but without droplets resting on or hanging from objects. One may use image editing techniques to add droplet images on these photographs using photo-enhancing software, such as Photoshop. Since a droplet reflects or

Regular Paper

Recommended by CAD/Graphcis 2019

This work was supported by the National Natural Science Foundation of China under Grant Nos. 61772463 and 61772440, the Aeronautical Science Foundation of China under Grant No. 20165168007, and the National Key Research and Development Program of China under Grant No. 2018YFB1700900.

refracts the light coming from the environment, forming a deformed image on the surface of the droplet, it is usually hard to find droplet photographs with the environment light consistent with those in the photographs without droplets. We can avoid this problem by integrating different media, such as images (original photographs) and graphics (3D virtual droplets), and augment original photographs with 3D virtual droplets. Such artistic augmentation of photographs offers many possibilities for potential creative applications, such as digital games and augmented reality. For instance, we can manipulate the shapes and positions of virtual droplets, or change the environment light, to obtain stunning picture effects.

In this paper we propose a framework for artistic augmentation of photographs with droplets. To our knowledge, this is the first attempt in developing a model directed toward this goal. To help users achieve their imaginative visual effects, we offer a set of tools for estimating the illuminating condition of the natural scene in the original photograph, modeling droplets either realistically or artistically, and changing the visual information on inserted droplet surfaces. Our contributions include: 1) a novel approach for artistic augmentation on an input image by using a new environment map and rendering virtual droplets onto the image, and 2) tools for users to effectively model hanging and resting droplets aesthetically.

2 Related Work

Our work broadly falls into the area of rendering virtual objects into photographs, and focuses on: 1) accurate calibration, 2) geometric consistency, and 3) estimation of lighting condition. Methods in this area are driven by a large number of applications, ranging from augmented reality to visual effects and product visualization[1]. Our work is on artistic augmentation of photographs, and bears similarities with rendering virtual objects into photographs, such as the aforementioned characteristics 1 and 3. It can be distinguished from this area as it offers editing features like modeling droplets and changing the visual information on droplets. To limit the scope, we could calibrate the camera and recover the geometry of the scene by using existing methods (see for example books[2,3] or surveys[4,5] on the topic). Here we review two subjects closely related to our work: estimation of lighting condition and modeling of droplets.

2.1 Estimation of Lighting Condition

Estimation of lighting condition is necessary to achieve visual consistency between virtual and real objects. Methods of estimating the lighting condition could be divided into the following three categories.

The first category contains the methods that capture a physically accurate model of the lighting condition in a scene. Debevec[6] putted a mirror ball in the real world to obtain omnidirectional high dynamic range (HDR) images. Via careful selection of exposure times, apertures, and neutral density filters, Stumpfel *et al.*[7] discussed techniques for direct HDR capture of the sky and sun illumination conditions in an outdoor scene. Banterle *et al.*[8,9] provided tools for expanding low dynamic range contents for the generation of HDR images by adopting inverse tone mapping algorithms. An interactive interface named envyLight was presented by Pellacini[10], on which users could quickly adjust lighting features with a small set of editing operations. Recently, Debevec *et al.*[11] proposed a light probe design that obtains a full dynamic range of illuminations from a single exposure, and estimates the intensity of multiple saturated light sources by solving a simple linear system.

The second category of methods exploits properties of the human visual system to produce perceptually plausible illumination models. By transferring color statistics[12], Reinhard *et al.*[13] proposed a simple and easily implemented method for inserting virtual objects into legacy photographs and videos. Khan *et al.*[14] presented a method for automatically replacing one material with another by approximating the incident illumination from a single HDR image. An algorithm for multiple lights detection that leverages the limitations of the human visual system was presented by Lopez-Moreno *et al.*[15], which could be adopted for image composition and virtual object insertion. By assuming the scene in a box, Karsch *et al.*[16] provided an interaction-based approach. They created a physical model of the scene suitable for rendering virtual objects with diffuse, specular, and even glowing materials while accounting for the interaction of lighting between objects and the scene. Furthermore, improving the method of [16], Karsch *et al.*[17] developed a user-friendly system that inserts non-specular objects into photographs of indoor scenes using the methods of [18] and [19] to estimate illumination.

The third category focuses on estimating physical illumination using the available prior information on the sky. Lalonde *et al.*[20] used the Perez sky model[21] as the prior information to estimate outdoor illumination. Furthermore, combining with other scene features, such as cast shadows, shading on vertical surfaces and convex objects, Lalonde *et al.*[22−24] developed methods for estimating natural illumination environment from a single image. Adopting a simple illumination model of outdoor scene, Liu *et al.*[25] assumed that the sun is a directional light source and the sky is a uniform area light source, thereby the illumination can be estimated with the illumination related statistical parameters or basis learned from sample images. Liu and Granier[26] adopted the same assumptions, and took spatial and temporal coherence of illumination to recover illumination from videos captured by moving cameras. Recently, Xing *et al.*[27] proposed a framework which simulates the environment illumination and projects complex shadows on the ground of the real scene to the surface of the virtual object.

Most photographs with droplets resting/hanging on objects are taken at a close range or with a long focal-length len, and thus only a little scene is included in the image. While droplets in the scene may reflect/refract other objects in the environment that are outside of the image, we need to select a new image as the environment map so that objects in the new environment map can be reflected/refracted on the droplet surfaces.

2.2 Modeling of Droplets

In most applications of rendering virtual objects into photographs, 3D virtual objects inserted into real-world images are rigid; thus their shapes remain unchanged in the scene. A water droplet is a small column of liquid, whose shape may vary in a considerable range when interacting with the surface of other objects. It is therefore necessary to model droplets with proper shapes according to where they are inserted in the image. Most previous models of droplets do not address this issue, since they serve other applications, such as animations. In order to present or calculate deformations of droplets caused by interactions with other objects, both droplets and other objects must be modeled in 3D. In our work, droplets are always static, and we therefore only review the work on droplet modeling, and omit those studies on physically-based fluid simulation.

The earliest droplet model is called metaball model[28], which is defined by a few simple constraints, and allows for simple free-form deformations. O'Brien and Hodgins[29] presented a method for modeling water spray using a particle system. Murta and Miller[30] developed several approaches to establish a means of portraying dynamic liquid behaviors, such as pouring and splashing within synthetic scenes. A method for modeling flowing droplets using a mass-spring system with the surface tension and volume conservation constraints was presented by Fournier *et al.*[31] In order to animate droplets and their streams on a glass plate realistically in a high speed, Kaneda *et al.*[32,33] proposed a discrete surface model of a glass plate and an efficient rendering method taking into account reflection and refraction of light. Later, Yu *et al.*[34] modeled static droplet shapes on flat surfaces using the metaball concept, and Tong *et al.*[35] presented a volume-preserving approach for liquids modelled by metaball.

Our goal is synthesizing realistic images and seamlessly merging 3D virtual droplets into real-world scenes in the form of 2D photographic images. To make virtual droplets look as natural as in the real world, we must take into account the objects on which hanging or resting droplets are added when modeling the droplets' shapes. Also, the artistic augmentation of images with droplets may require droplets in a large quantity, thereby we aim at providing users with a simple means of generating droplet models in such a situation.

3 Approach Overview

The overall architecture of our framework is presented in Fig.2. The first part of our framework includes illumination condition estimation and environment map adjustment. The first stage of this part is geometry and sunlight estimation (the green box). This includes estimating the scene depth or approximating objects with simple models, and estimating camera parameters and the direction of sunlight. The next stage is material and illumination initialization (the light blue box), i.e., initializing parameters of sunlight, environment light and scene materials by solving a linear equation system of the illumination model. We then recover the final parameters of sunlight, environment light and scene materials by an iteration procedure, starting from the initial parameters (the dark blue box). In the stage of environment map adjustment (the gray box), we select a new image as the environment map, and adjust the brightness and colors in the environment map with the radiance of the environment light estimated from the input image.

The second part of our framework is modeling of

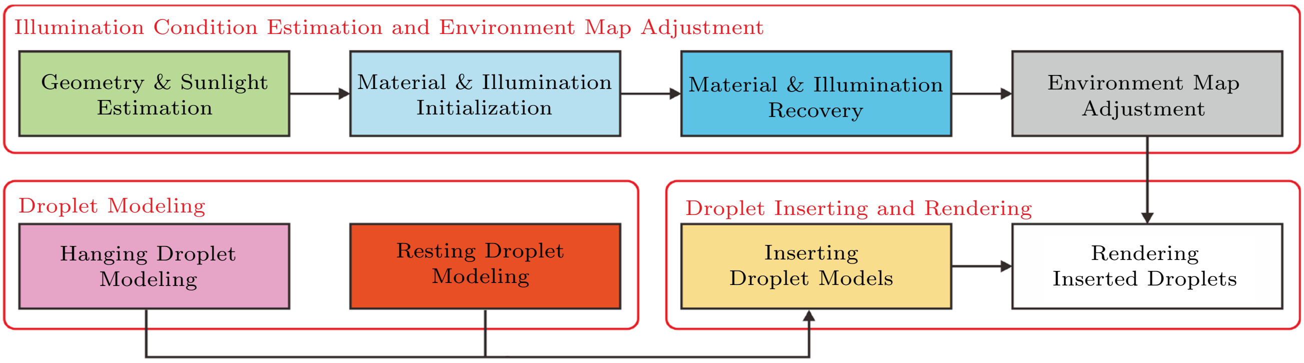

Fig.2. Framework for artistic augmentation of photographs with water droplets.

droplets. The framework offers two means for generating 3D droplet models. One is hanging droplet modeling based on geometric constraints (the pink box). The other is resting droplet modeling based on binary images of strokes with droplet shapes drawn (the red box).

The third part of our framework includes inserting 3D droplet models (the yellow box) and rendering the inserted models with the adjusted environment map (the white box). The following sections describe our system in detail.

4 Estimation of Illumination Conditions

In most applications of rendering virtual objects into photographs, estimating illumination conditions in a real-world scene aims at rendering virtual objects with shading and shadows consistent with the lighting conditions. Once the environment light is obtained from the real-world scene, it is used as an environment map to render the virtual objects. As suggested in [36], most of real-world surfaces exhibit a mixture of interface reflection (specular reflection) and body reflection (diffusion reflection). To estimate outdoor illumination conditions[22,27,37], we can use the following model. For a point p in the scene of the input image $\mathcal{I}$, if we model the sunlight as the directional light with irradiance $E^{\rm sun}$ and direction $\boldsymbol{l}$, and the environment light as the ambient light with irradiance $E_p^{\rm env}$ at point p, the trichromatic (R,G,B channels) color of point p could be expressed as

$$I_p = (\rho_p(\boldsymbol{n}_p \cdot \boldsymbol{l}) + k_p(\boldsymbol{n}_p \cdot \boldsymbol{h}_p)^{\alpha_p})s_p^{\rm sun}E^{\rm sun} + \rho_p s_p^{\rm env}E_p^{\rm env}, \quad (1)$$

where $s_p^{\rm sun} \in [0,1]$ and $s_p^{\rm env} \in [0,1]$ are the sunlight occlusion coefficient and the environment light occlusion coefficient respectively, ρ_p is the diffuse coefficient, k_p and α_p denote the specular properties, $\boldsymbol{n}_p$ is the surface normal at p, and $\boldsymbol{h}_p$ denotes the half-vector between $\boldsymbol{l}$ and the viewing direction.

Some of the recent studies aimed at recovering whole-environment map based on a single image[38−40]. They, however, usually require the input image $\mathcal{I}$ to cover large portions of the scene[22]; thus they are unsuitable for our applications where only a small portion of the scene is covered in $\mathcal{I}$ (because input images are usually taken at a close range or with a long focal-length len). Considering that the virtual droplets may reflect large portions of the scene uncovered in the image, we use a new image $\mathcal{I}'$ to construct the environment map. However, mismatches of brightness and colors between $\mathcal{I}'$ and $\mathcal{I}$ may cause rendered droplets with brightness and colors inconsistent with those in $\mathcal{I}$. It is thus necessary to adjust the brightness and colors of $\mathcal{I}'$ to ensure the illumination and color consistency between $\mathcal{I}'$ and $\mathcal{I}$. We propose a simple solution to this problem as described below.

Our idea is to first estimate the irradiance of the environment light ($E_p^{\rm env}$ in (1)) in the scene from the cues of the input image $\mathcal{I}$, and then adjust the brightness and colors of $\mathcal{I}'$ using the estimated $E_p^{\rm env}$.

4.1 Geometry Estimation

To insert natural-looking droplets into photographs, we need to calibrate the camera and estimate the coarse geometry of the scene (depicted in the photograph) to model lighting effects. The camera could be calibrated by using the method proposed in [41]. To estimate the coarse geometry, considering that objects in the input image are usually simple in structure, such as the lotus bud, lotus leaves and tree branches, we can use simple models, such as a spindle shape, a plane, or a cylinder, to approximate their 3D structures. Once a model is adopted, the surface normal $\boldsymbol{n}_p$ in (1) can be obtained as shown in Fig.3.

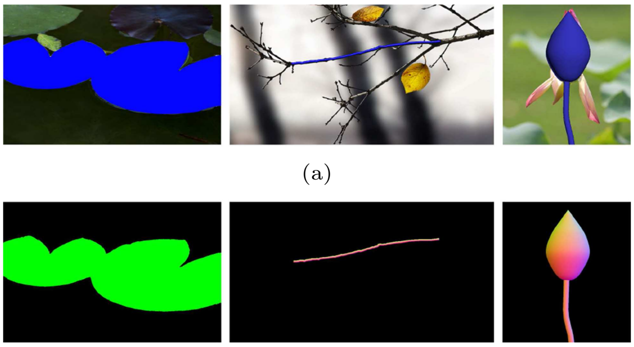

(a)

(b)

Fig.3. Approximating the 3D structures using (a) simple models and (b) corresponding normal maps.

4.2 Sunlight Direction Estimation

The sunlight direction should be estimated from the input image $\mathcal{I}$ so that virtual droplets could be rendered with consistent shading and shadows. Although an automatic approach was proposed by Lalonde *et al.*[23] to estimate the sun's position based on a single outdoor image using Perez's sky model, it requires sufficient cues, such as the sky, shadows, and multiple vertical planes (e.g., buildings and walls) in the scene, to make a reasonable estimation. In our applications, the input image, typically of a small scene, is assumed to contain limited or no cues, thereby we ask the user to estimate and adjust the direction of sunlight $\boldsymbol{l}$ in (1) interactively by observing the generated results.

4.3 Material and Illumination Initialization

In many cases including both sunny days and cloudy days, it is reasonable to assume that the environment light is distributed uniformly[25,42,43]; thus we have $E_p^{\mathrm{env}} = L^{\mathrm{env}} \int_\Omega (\boldsymbol{n}_p \cdot \boldsymbol{e}_\omega)\mathrm{d}\omega$, where Ω is the hemisphere above p, L^{env} is the radiance of the incident light, and $\boldsymbol{e}_\omega$ is the unit vector of direction ω. Let C_p denote the known part, $C_p = \int_\Omega (\boldsymbol{n}_p \cdot \boldsymbol{e}_\omega)\mathrm{d}\omega$, then $E_p^{\mathrm{env}} = L^{\mathrm{env}} C_p$.

Our applications involve materials of weak specular reflectance, such as lotus leaves and tree branches. Similar to Boivin and Gagalowicz's method[44], we start the algorithm by assuming the surface to be perfectly diffused when obtaining the initial illumination parameters E_0^{sun}, L_0^{env}, and a material parameter $\rho_{p,0}$. The final parameters of illumination and materials are then obtained by an iteration procedure described in Subsection 4.4.

Ignoring the specular component in (1), we could simplify the illumination model as

$$I_p = (\boldsymbol{n}_p \cdot \boldsymbol{l})\rho_p s_p^{\mathrm{sun}} E^{\mathrm{sun}} + \rho_p s_p^{\mathrm{env}} C_p L^{\mathrm{env}}, \qquad (2)$$

where the surface normal $\boldsymbol{n}_p$ and the sunlight direction $\boldsymbol{l}$ are known (Subsection 4.1 and Subsection 4.2 respectively). We set the occlusion coefficients with $s_p^{\mathrm{sun}} = 1$ and $s_p^{\mathrm{env}} = 1$ as suggested in [26]. The remaining unknown variables in (2) are E^{sun}, L^{env} and ρ_p. Inspired by Bousseau *et al.*'s work[45], we let the user choose points in the scene $\mathcal{I}$ which share the same material (i.e., the same ρ_p) using a brush tool as shown in Fig.4. When n points are chosen and put into Φ, there are $3n$ equations (in R, G, B channels respectively). The number of unknown variables is reduced dramatically since the points chosen share the same material.

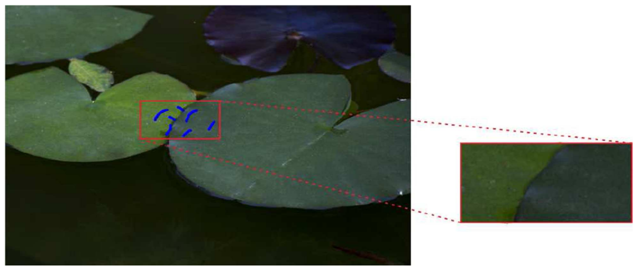

(a) (b)

Fig.4. The user-drawn blue strokes indicate that the covered points in the scene share the same material. The recovered diffused albedo of points of the leaves is shown in (b).

Furthermore, to improve the estimation accuracy, we employ additional constraints, such as $E^{\mathrm{sun}}(R) > E^{\mathrm{sun}}(G) > E^{\mathrm{sun}}(B)$ for the sunlight, and $L^{\mathrm{env}}(R) < L^{\mathrm{env}}(G) < L^{\mathrm{env}}(B)$ for the environment light, as suggested in [27]. The initial illumination parameters E_0^{sun} and L_0^{env}, and the material parameter $\rho_{p,0}$ can be obtained by solving this linear system of equations using linear constrained least squares.

4.4 Material and Illumination Recovery

To calculate the material parameters (ρ_p, k_p and α_p) in (1) by the information provided by the points in Φ, we set α_p to 1 and assume that the specular properties of the surface covered by points in Φ change slowly. Using the initial illumination parameters obtained in Subsection 4.3, we solve ρ_p and k_p by the following iterative objective function:

$$\begin{aligned} \arg \min_{\rho_{p,i}, k_{p,i}} \sum_{p \in \Phi} & |I_{p,i} - \mathcal{I}_p|^2 + \gamma_1 m_{p,i} |\nabla \rho_{p,i}|^2 + \\ & \gamma_2 |\rho_{p,i} - \rho_{p,i-1}|^2 + \gamma_3 |\nabla k_{p,i}|^2 \\ \text{subject to} \quad & 0 \leqslant \rho_{p,i} \leqslant 1,\ 0 \leqslant k_{p,i} \leqslant 1, \end{aligned} \qquad (3)$$

where γ_1, γ_2, γ_3 are weights, and set to 5.0, 3.0, 5.0 respectively through experiments. $m_{p,i}$ is defined as $m_{p,i} = 1 - 1/(1 + e^{-s(|\nabla I_{p,i}|^2 - c)})$ with settings $s = 10.0$, $c = 0.15$ to penalize the pixels with large gradient magnitudes[16]. The first term ensures $I_{p,i}$ to conform with $\mathcal{I}_p$, the second term enforces the smoothness of albedo, and the remaining terms ρ_p and k_p are piecewise constants.

Next we update the illumination parameters (E^{sun} and L^{env}) in the illumination model defined in (3) to obtain $\rho_{p,i}$ and $k_{p,i}$. Similar to the estimation of the environment light in Subsection 4.3, adopting the color constraints again, we plug $\rho_{p,i}$ and $k_{p,i}$ into the following iterative objective function

$$\begin{aligned} \arg\min_{E_i^{\mathrm{sun}}, L_i^{\mathrm{env}}} & \sum_{p \in \Phi} (\rho_{p,i}(\boldsymbol{n}_p \cdot \boldsymbol{l}) + k_{p,i}(\boldsymbol{n}_p \cdot \boldsymbol{h}_p)^{\alpha_p}) \times \\ & s_p^{\mathrm{sun}} E_i^{\mathrm{sun}} + \rho_{p,i} s_p^{\mathrm{env}} C_p L_i^{\mathrm{env}} - \mathcal{I}_p \qquad (4) \\ \text{subject to} \quad & E_i^{\mathrm{sun}}(R) > E_i^{\mathrm{sun}}(G) > E_i^{\mathrm{sun}}(B), \\ & L_i^{\mathrm{env}}(R) < L_i^{\mathrm{env}}(G) < L_i^{\mathrm{env}}(B). \end{aligned}$$

The illumination parameters E_i^{sun} and L_i^{env} in the i-th iteration could also be instantiated by the method of linear constrained least squares. Let $err_i = |E_i^{\mathrm{sun}} - E_{i-1}^{\mathrm{sun}}|^2 + |L_i^{\mathrm{env}} - L_{i-1}^{\mathrm{env}}|^2$ indicate the error between two iterations and T denote the threshold. The iteration terminates when $err_i \leqslant T$ and the final estimated parameters (ρ_p, k_p, E^{sun} and L^{env}) are obtained. The algorithm for recovering the material and illumination parameters is given in the following pseudo-code (see Algorithm 1).

Algorithm 1. Iteration of Illumination and Material Recovering

Input: initialized parameters E_0^{sun}, L_0^{env} and $\rho_{p,0}$

Output: final material parameters ρ_p, k_p and illumination information L^{env}, E^{sun}

for: $i \Leftarrow 1$; $err_i > th$; $i \Leftarrow i + 1$ **do**

  $\rho_{p,i}$, $k_{p,i} \Leftarrow$ Solving (3) with E_{i-1}^{sun}, L_{i-1}^{env} and $\rho_{p,i-1}$ as input

  E_i^{sun}, $L_i^{\mathrm{env}} \Leftarrow$ Solving (4) with $\rho_{p,i}$ and $k_{p,i}$ as input

  $err_i \Leftarrow |E_i^{\mathrm{sun}} - E_{i-1}^{\mathrm{sun}}|^2 + |L_i^{\mathrm{env}} - L_{i-1}^{\mathrm{env}}|^2$

end

4.5 Environment Light Adjustment

Next, we select a new HDR panorama image as the environment map, and adjust its brightness and colors with the radiance of the environment light L^{env} (obtained in Subsection 4.4) in the input image $\mathcal{I}$. We construct a temporal scene to have the same geometry and E^{env} with those in $\mathcal{I}$ but with a new environment light distribution $L_p'^{\mathrm{env}}$ in $\mathcal{I}'$. The irradiance of environment light at point p in this temporal scene is $E_p'^{\mathrm{env}} = \int_{\Omega(p)} L_p'^{\mathrm{env}}(\omega)(\boldsymbol{n}_p \cdot \boldsymbol{e}_\omega)\,\mathrm{d}\omega$, where $\Omega(p)$ is the upper hemisphere, and $\boldsymbol{e}_\omega$ is the unit vector of direction ω. The integral can be approximated by adopting spherical harmonics Y_{lm}[46], with $l \geqslant 0$ and $-l \leqslant m \leqslant l$, where l is set to 2, as suggested in [47, 48], and $E_p'^{\mathrm{env}}$ can be represented by

$$E_p'^{\mathrm{env}} = \sum_{l,m} \hat{A}_l L_{lm} Y_{lm}(\boldsymbol{n}_p), \qquad (5)$$

where $\hat{A}_l = \sqrt{\frac{4\pi}{2l+1}} A_l$ in which A_l is related to coefficient $A = (\boldsymbol{n}_p \cdot \boldsymbol{e}_\omega)$, and given numerically in [49]. L_{lm} are the lighting coefficients in the spherical harmonic basis function (5),

$$L_{lm} = \int_{\theta=0}^{\pi} \int_{\phi=0}^{2\pi} L(\theta, \phi) Y_{lm}(\theta, \phi) \sin\theta \,\mathrm{d}\theta \,\mathrm{d}\phi,$$

where θ is the zenith angle, and ϕ is the azimuth angle. The integrals could be viewed simply as the sum of the pixels in the environment map $\mathcal{I}'$, weighted by the functions of spherical harmonics $Y_{lm}(\theta, \phi)$.

We calculate a parameter μ by the following objective function:

$$\arg\min_{\mu(\lambda)} \sum_{p \in \Phi} |\mu(\lambda) E_p'^{\mathrm{env}}(\lambda) - C_p L^{\mathrm{env}}(\lambda)|^2,$$

where λ denotes the R, G, B channels. We then adjust the brightness and colors of $\mathcal{I}'$ by multiplying every pixel in $\mathcal{I}'$ by μ to obtain a new image which could be used as the environment map to render the virtual droplets. Fig.5 shows the synthetic images adopting $\mathcal{I}'$ as the environment map with and without the color and brightness adjustments.

(a) (b)

Fig.5. Comparison of rendered water droplets (b) with and (a) without adjustments of brightness and colors in the environment map.

5 Droplet Modeling

Our goal is to synthesize realistic images and seamlessly merge 3D virtual droplets into real-world scenes in the form of 2D photographic images. In most cases, droplets either rest or hang on other objects, and thus exhibit different shapes influenced by the water surface tension and gravity. Here we simulate droplet shapes by simple models and start from the hanging droplet model.

5.1 Hanging Droplet

We construct an initial droplet model as a hemisphere characterized by m radial slices, and n horizontal circular cross sections, with a radius r set at level 1, and the apex point, as illustrated in Fig.6. The model consists of $mn + 1$ points, represented by the spherical coordinates $q(r, \alpha, \beta)$. Next we describe how to deform this initial droplet model to obtain the shape of a hanging droplet.

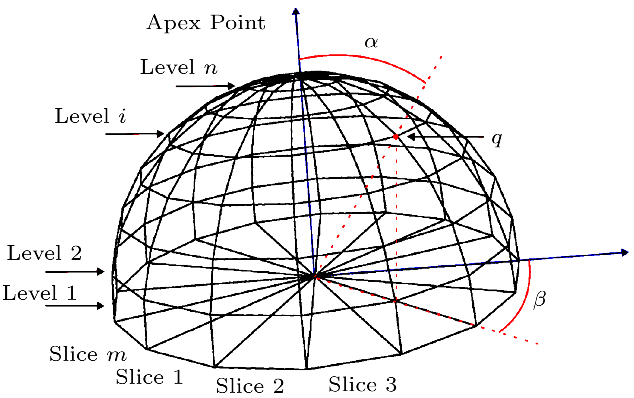

Fig.6. Initial un-deformed hanging droplet model.

Accurate modeling of hanging droplet shapes is difficult, because a hanging droplet is produced when equilibrium is attained between the interfacial energies (liquid, air and solid surface) and gravity, and its shape also depends on its size[50]. Based on our observation of hanging droplets in artistic photography, we deform the outline of our initial droplet model into a bell-shaped curve, as illustrated by the red line in Fig.7(a). This bell-shaped curve can be approximated simply by $r_i = |\frac{r}{\pi}\arcsin(2\cos\alpha - 1) - \frac{r}{2}|$, where r_i is the radius at the i-th level, as illustrated in Fig.7(b).

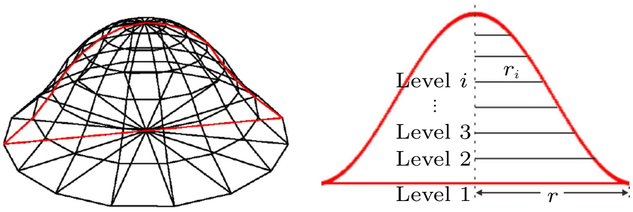

(a) (b)

Fig.7. Deformed hanging droplet model. (a) A bell-shaped model. (b) Cross section of the bell-shaped model.

To enable user control over the hanging droplet shape, such as a vertically elongated droplet, we use a parameter $w_i = 1 + (\epsilon - 1)\cos\alpha_i$, $\epsilon \in [1, 2]$ to adjust the radius at each level, i.e., $r_i = w_i|\frac{r}{\pi}\arcsin(2\cos\alpha - 1) - \frac{r}{2}|$. The smaller the value ϵ is, the longer the droplet becomes, as shown in Fig.8.

(a) (b) (c)

Fig.8. Droplets hanging from the surface with following parameter settings: (a) $\epsilon = 2.0$, (b) $\epsilon = 1.6$, and (c) $\epsilon = 1.2$.

5.2 Resting Droplets

Modeling droplets resting on other objects is also a very challenging task, because the droplet shapes depend on the static contact angle and droplet volume[51]. A droplet's shape is of great relevance to the interaction of the droplet with the interface. Small droplets have spherical or hamburger bun shapes, but as they grow larger and rest on an irregular surface, their interaction with the interface becomes stronger, leading to irregular droplet formation[52]. Our goal is the artistic augmentation of photographs, which may contain a large number of droplets, thereby traditional droplet modeling methods are laborious and time-consuming in such situation.

Inspired by [53] and [54], we propose a simple image based approach for modeling resting droplets. Compared with 3D modeling of droplets, it is easier for users or artists to draw strokes of different shapes in 2D.

Our user interface allows users to input a binary image I_s drawn with white strokes, as shown in white regions in Fig.9(a). Next, we apply distance transformation to those white regions in I_s to obtain a distance map (Fig.9(b)). However, such a distance map cannot be used straightforwardly as the height map of droplets, because the gray values of the points inside white regions are changed to show linear slopes of ridges in the distance map (better seen in its corresponding mesh model, in Fig.9(c)). In order to make those ridge slopes look curvy in the height map so that the heights of droplets can be approximated naturally, we raise the grey value of each point in the distance map to the power of n, and the resultant image I_h is shown in Fig.9(d) with parameter settings from left to right: $n = 2, n = 3, n = 4$. The larger n is, the flatter the droplet becomes. We set $n = 4$ as default through experiments. In order to smooth ridges in I_h (better seen in I_h's corresponding mesh model (Fig.9(e)), we apply the Gaussian filter to I_h and obtain I_g as shown in Fig.9(f). To remove the "leakage" outside of the stroke shapes caused by the Gaussian filering, we employ I_s as a binary mask, and perform the operation $I'_g = I_g \odot I_s$, where $\odot$ is the Hadamard product. Finally, we convert the height map I'_g to mesh models and render these models to obtain droplets with different n settings, as shown in Fig.9(h).

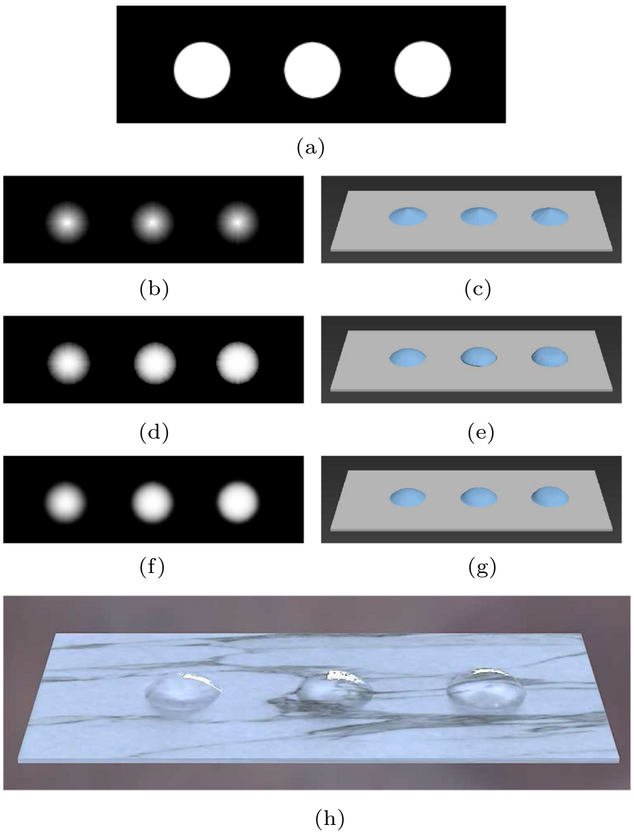

Fig.9. Image-based droplet modeling. (a) Hand-drawn droplet shapes. (b) Distance map of white regions in (a). (c) 3D droplet models corresponding to (b). (d) Raising the grey value of each point in (b) with the following parameter settings from left to right $n = 2, n = 3, n = 4$. (e) 3D droplet models corresponding to (d). (f) Resulting image of (d) smoothed by a Gaussian filter. (g) 3D droplet models corresponding to (f). (h) Rendered 3D droplets.

6 Adding Virtual Droplets

Artistic augmentation of photographs with droplets requires various input parameters, such as the number, sizes and shapes of droplets, and their locations in the given scene. When proper virtual droplets are added into the input image $\mathcal{I}$ using Debevec's method[6], we render them by V-Ray renderer① to obtain two images. One image $\mathcal{I}_{\text{aug}}$ contains the scene augmented with droplets, the other image $\mathcal{I}_{\text{naug}}$ contains the original scene, and both are illuminated by the sunlight and environment light. Let M be an object mask which is a scalar image equaling 0 on pixels outside the projected area of droplets, and $(0, 1]$ on other pixels. The final synthetic image $\mathcal{I}_f$ could be generated by

$$\mathcal{I}_f = M \odot \mathcal{I}_{\text{aug}} + (1 - M) \odot (\mathcal{I}_{\text{aug}} + \mathcal{I} - \mathcal{I}_{\text{naug}}).$$

7 Results and Discussions

Our system is implemented using Microsoft Visual C++, OpenGL Mathematics, GNU Scientific Library②, Qt 5.70, and runs on a PC with 3.3 GHz CPU (Inter® Core i5-4590), 16 GB memory and NVIDIA GeForce GTX 960. This section shows several examples of artistic augmentation of images with droplets. In the first three examples we add virtual droplets on photographic images and the last example presents a different visual effect created by our droplet augmentation method.

Fig.10 shows an example in which we add virtual droplets to the lotus leaves originally without droplets. The virtual droplets are rendered with the environment map shown at the bottom left corner of Fig.10(a). Those rendered droplets are sparkle and their shadows are cast on lotus leaves.

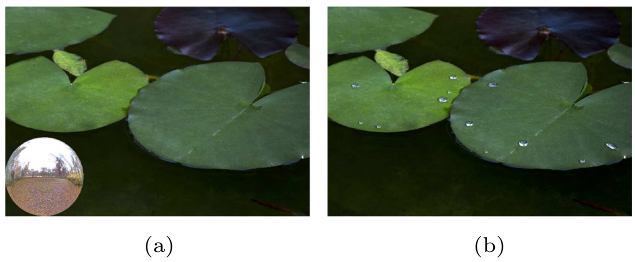

Fig.10. Artistic augmentation of lotus leaves with droplets. (a) Input image without droplets and the environment map at the bottom left corner. (b) Augmented lotus leaves with droplets.

In the second example we add virtual droplets on the lotus bud (Fig.11). In this example, we use a cylinder to approximate the 3D structure of the lotus stalk. In the stage of illumination recovery, we choose a few points of the same material on the lotus stalk in the image to estimate the illumination condition. We then

①Group G. V-ray. https://www.chaosgroup.com/vray/sketchup, March 2018.

②GNU. Gls. http://www.gnu.org/software/gsl, March 2018.

take a spindle shape to approximate the geometry of the lotus bud and add a few droplets on the lotus bud surface. We finally render those added droplets with the environment map shown at the bottom left corner of Fig.11(a) (sunset with clouds above the sea). Fig.11(b) shows the augmented lotus bud.

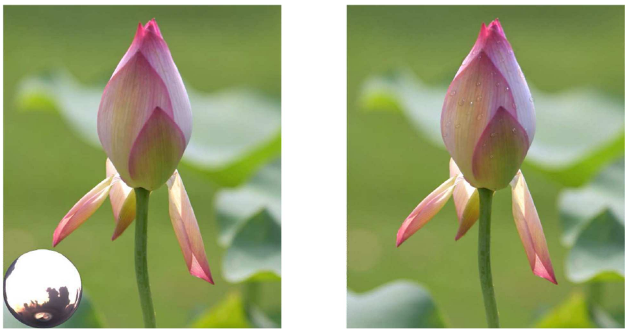

(a) (b)

Fig.11. Artistic augmentation of the lotus bud with droplets. (a) Input image without droplets and the environment map at the bottom left corner. (b) Augmented lotus bud with droplets.

Fig.12 presents the third example in which we add droplets hanging from branches. In this case, it is unnecessary to know the whole geometry of branches, because we only need to recover a small part of the branches' geometry (in Fig.3) to estimate the environment parameters. We then place hanging droplets in the desired positions in the input image (Fig.12(a)), and render them using the environment map shown at the bottom left corner of Fig.12(a). Please note that hanging droplets refract rather than reflect the environmental lighting, thus forming an up-side down image of the environment map on the droplet surfaces, as shown in Fig.12(b) and Fig.12(c).

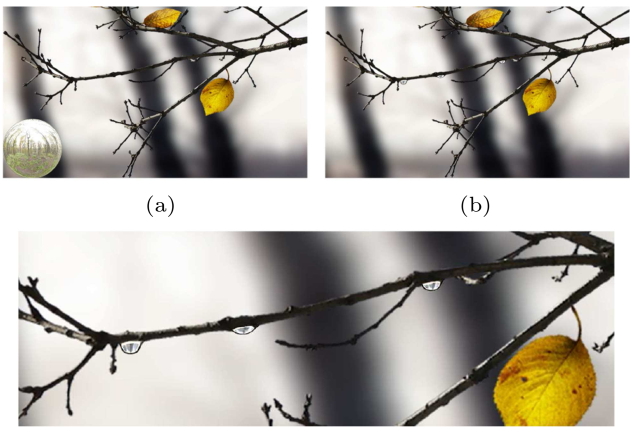

(a) (b)

(c)

Fig.12. Artistic augmentation of tree branches with hanging droplets. (a) Input image without droplets and the environment map at the bottom left corner. (b) Augmented branches with droplets. (c) Enlarged local view of (b).

To measure the time involved in the user interactions, we conduct a user study to evaluate the average time spent on interactions, such as geometry estimation, sunlight direction estimation, illumination recovery and adding droplets. Twenty volunteers (14 male and 6 female, aged of 20–27) are recruited for this task. Our test adopts three different scenes (lotus leaves in Fig.10, the lotus bud in Fig.11 and tree branches in Fig.12), and the average time spent on those interactions is shown in Table 1. For the scene of the lotus bud, users take a longer time on the step of adding droplets because more droplets need to be added. Nevertheless, the duration for these interactions is reasonable for AR applications.

Table 1. Average Time Spent on Interactions

	Geometry (s)	Sunlight Direction (s)	Illumination (s)	Adding Droplets (min)
Fig.10	2.4	23.5	61.2	< 1
Fig.11	11.7	31.6	57.7	< 4
Fig.12	6.1	27.8	64.8	< 1

We also adopt different HDR panorama images as the environment map for the same input image as shown in Fig.13(a), so that different environment maps could be reflected or refracted on the droplet surfaces. Thus our method extends the design space for users to select different environment maps as desired to obtain stunning effects. Although in Xing *et al.*'s method[27], the sky model[21] could be added when the input image has a large open area, such as land or water, the rendered droplets reflect or refract mainly the visual information in the sky, as shown in Fig.13(b), which looks rather dull and uninteresting compared with previous three rendered results.

Apart from the artistic augmentation of photographic images, our system is also able to generate special visual effects, which requires only a hand-drawn template, as demonstrated by the following example.

According to the principle of similarity in Gestalt theory[55], the perception lends itself to seeing stimuli that physically resemble each other as part of the same object, and stimuli that are different as part of a different object. It is possible then for us to use droplets of distinctive sizes to depict different objects in an image, as demonstrated by an example in Fig.14(d). The figure depicts decorative tree images on a window glass by three kinds of stimuli: tiny droplets suggesting foggy effect on the glass, bigger droplets depicting several tree trunks, and the blank space depicting several thick trunks and leaves.

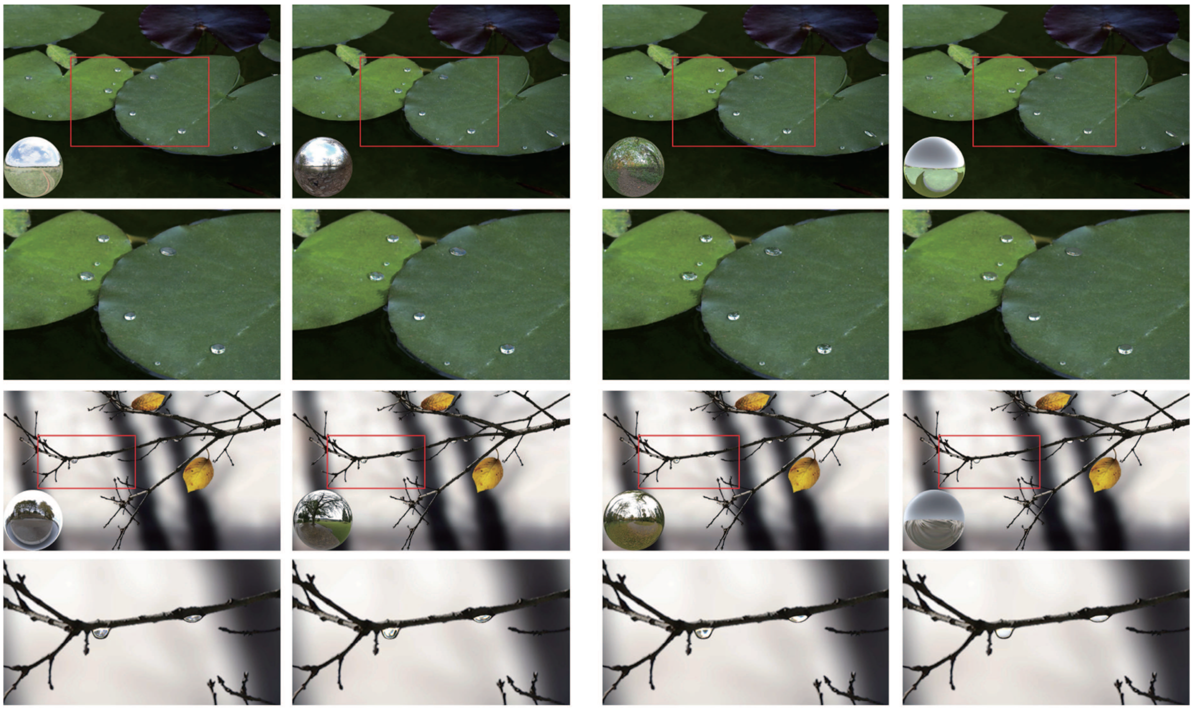

(a) (b)

Fig.13. Visual comparison with Xing *et al.*'s method[27]. (a) Synthetic images and corresponding enlarged parts by our method with different environment maps. (b) Synthetic images and corresponding enlarged parts by Xing *et al.*'s method[27].

(a) (b) (c)

(d)

Fig.14. Decorative tree images depicted with droplets of varying sizes on a window glass. (a) Hand-drawn template of decorative tree images. (b) Gloss map of the window glass. (c) Input background image. (d) Final rendered result.

In this example, we first ask an artist to draw a template of decorative tree images, as shown in Fig.14(a), in which black, gray and white regions can be used as sub-templates denoted by T_b, T_g and T_w, respectively. Taking gray regions for instance, we generate a random dot like a stroke pattern of proper sizes in a window of the same size as the input scene picture and denote it as P_g. We perform the Hadamard product between T_g and P_g to obtain a stroke pattern depicting shapes of gray regions in Fig.14(b). The resulting stroke pattern is then converted into the droplet model using the method described in Subsection 5.2. For black regions in Fig.14(a), we place random dots as tiny droplets in them. We leave white regions in Fig.14(a) without painting anything on them.

During the rendering phase, we place a night scene image as the background (Fig.14(c)), and render the droplet models in the gray regions in Fig.14(a) with a few simple lights. To reduce the rendering time, we do not convert random dots in the black regions into mesh models. Instead, we take random dots as the gloss map to set the refraction glossiness for the window glass. The gloss map for white regions is in black, indicating that no refraction occurs. After these regions are rendered, we synthesize them with the regions of droplets to obtain the final result (Fig.14(d)).

A user study was conducted to evaluate whether the artistically augmented photographs look better than the original photographs. Forty volunteers (24 male and 16 female, aged between 20 and 27) were recruited as the subjects for this task. Our test adopted five different scenes (the first four are shown in Figs.10–14 respectively, and the fifth is shown in Fig.15(b)), which were presented in a randomly permuted order. For each scene, the original image and the synthetic image produced by our method were demonstrated, and image placement was also randomized. The subjects were asked to select the image that looks more artistic and appealing. The results of the user study are shown in Fig.15(a), revealing that the majority of users think that synthetic images with droplets are more artistic and appealing than the original ones.

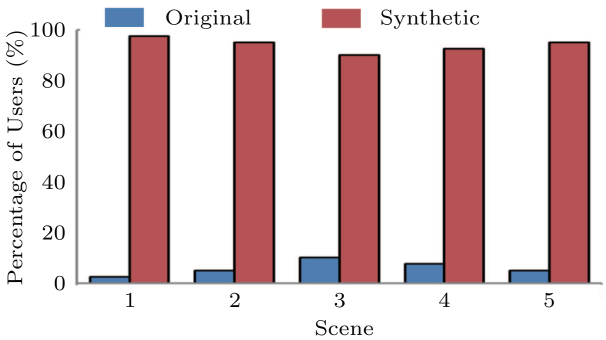

(a)

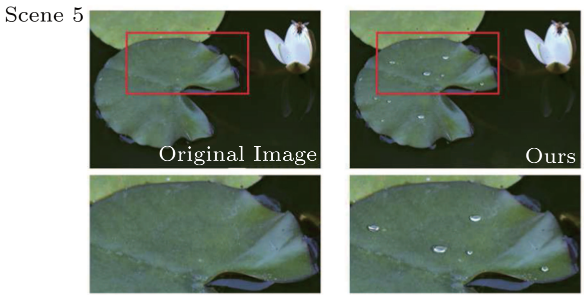

(b)

Fig.15. We propose a user study to evaluate whether the artistically augmented photographs look better than the original photographs. (a) Results of the user study. For each scene, the bars of two different colors represent the percentage of users who select more artistic and appealing images between the original (blue) and synthetic (red) image. (b) The 5th scene in the user study.

8 Conclusions

This paper presented a novel approach to artistic augmentation of photographic images with droplets. Our work differs from traditional methods in that the environment map cannot be constructed straightforwardly from the input images. We instead selected a new image to construct the environment map and studied a key problem arising from the change of the environment map — ensuring the illumination consistency between the new environment map and the original input image. We proposed a method of environment map adjustment by using the radiance of the environment light estimated from the input image.

Furthermore, we proposed two means for generating 3D droplet models: one is hanging droplet modeling based on geometric constraints, and the other is resting droplet modeling based on binary images of strokes with droplet shapes drawn.

Potential applications of our work range from advertisements, posters, postcards, packaging, gaming, to special effects in digital art. As future work, we plan to augment images by animating virtual droplets, and this requires the recognition of objects and moving droplets along the recognized objects.

Acknowledgements We would like to thank the associate editor and all the reviewers for their constructive comments that have helped us to improve the presentation.

References

[1] Kronander J, Banterle F, Gardner A, Miandji E, Unger J. Photorealistic rendering of mixed reality scenes. *Comput. Graph. Forum*, 2015, 34(2): 643-665.

[2] Hartley R I, Zisserman A. Multiple View Geometry in Computer Vision (2nd edition). Cambridge University Press, 2004.

[3] Schmalstieg D, Höllerer T. Augmented Reality: Theory and Practice (1st edition). Addison-Wesley Professional, 2016.

[4] van Krevelen D W F, Poelman R. A survey of augmented reality technologies, applications and limitations. *The International Journal of Virtual Reality*, 2010, 9(2): 1-20.

[5] Rabbi I, Ullah S. A survey of augmented reality challenges and tracking. *ACTA GRAPHICA*, 2013, 24(1/2): 29-46.

[6] Debevec P. Rendering synthetic objects into real scenes: Bridging traditional and image-based graphics with global illumination and high dynamic range photography. In *Proc. the 25th Annual Conference on Computer Graphics and Interactive Techniques*, July 1998, pp.189-198.

[7] Stumpfel J, Tchou C, Jones A, Hawkins T, Wenger A, Debevec P. Direct HDR capture of the sun and sky. In *Proc. the 3rd International Conference on Computer Graphics*, November 2004, pp.145-149.

[8] Banterle F, Ledda P, Debattista K, Chalmers A. Inverse tone mapping. In *Proc. the 4th International Conference on Computer Graphics and Interactive Techniques*, November 2006, pp.349-356.

[9] Banterle F, Debattista K, Artusi A, Pattanaik S, Myszkowski K, Ledda P, Chalmers A. High dynamic range imaging and low dynamic range expansion for generating HDR content. *Computer Graphics Forum*, 2009, 28(8): 2343-2367.

[10] Pellacini F. Envylight: An interface for editing natural illumination. *ACM Transactions on Graphics*, 2010, 29(4): Article No. 34.

[11] Debevec P, Graham P, Busch J, Bolas M. A single-shot light probe. In *Proc. the 39th International Conference on Computer Graphics and Interactive Techniques*, August 2012, Article No. 10.

[12] Reinhard E, Ashikhmin M, Gooch B, Shirley P. Color transfer between images. *IEEE Computer Graphics and Applications*, 2001, 21(5): 34-41.

[13] Reinhard E, Akyuz O A, Colbert M, Hughes C, O'Connor M. Real-time color blending of rendered and captured video. In *Proc. Interservice/Industry Training, Simulation and Education Conference,* Dec. 2004, Article No. 1502.

[14] Khan E A, Reinhard E, Fleming R W, Bülthoff H H. Image-based material editing. *ACM Transactions on Graphics*, 2006, 25(3): 654-663.

[15] Lopez-Moreno J, Hadap S, Reinhard E, Gutierrez D. Compositing images through light source detection. *Computers & Graphics*, 2010, 34(6): 698-707.

[16] Karsch K, Hedau V, Forsyth D, Hoiem D. Rendering synthetic objects into legacy photographs. *ACM Transactions on Graphics*, 2011, 30(6): Article No. 157.

[17] Karsch K, Sunkavalli K, Hadap S, Carr N, Jin H, Fonte R, Sittig M, Forsyth D. Automatic scene inference for 3D object compositing. *ACM Transactions on Graphics*, 2014, 33(3): Article No. 32.

[18] Grosse R, Johnson M K, Adelson E H, Freeman W T. Ground truth dataset and baseline evaluations for intrinsic image algorithms. In *Proc. the 12th IEEE International Conference on Computer*, September 2009, pp.2335-2342.

[19] Achanta R, Shaji A, Smith K, Lucchi A, Fua P, Süsstrunk S. SLIC superpixels compared to state-of-the-art superpixel methods. *IEEE Transactions on Pattern Analysis & Machine Intelligence*, 2012, 34(11): 2274-2282.

[20] Lalonde J F, Efros A A, Narasimhan S G. Webcam clip art: Appearance and illuminant transfer from time-lapse sequences. *ACM Transactions on Graphics*, 2009, 28(5): Article No. 131.

[21] Perez R, Seals R, Michalsky J. All-weather model for sky luminance distribution — Preliminary configuration and validation. *Solar Energy*, 1993, 50(3): 235-245.

[22] Lalonde J F, Efros A A, Narasimhan S G. Estimating natural illumination from a single outdoor image. In *Proc. the 12th IEEE International Conference on Computer Vision*, September 2009, pp.183-190.

[23] Lalonde J F, Efros A A, Narasimhan S G. Estimating the natural illumination conditions from a single outdoor image. *International Journal of Computer Vision*, 2012, 98(2): 123-145.

[24] Lalonde J F. Understanding and recreating visual appearance under natural illumination [Ph.D. Thesis]. Carnegie Mellon University, 2011.

[25] Liu Y, Qin X, Xu S, Nakamae E, Peng Q. Light source estimation of outdoor scenes for mixed reality. *The Visual Computer*, 2009, 25(5/6/7): 637-646.

[26] Liu Y, Granier X. Online tracking of outdoor lighting variations for augmented reality with moving cameras. *IEEE Transactions on Visualization and Computer Graphics*, 2012, 18(4): 573-580.

[27] Xing G, Zhou X, Peng Q, Liu Y, Qin X. Lighting simulation of augmented outdoor scene based on a legacy photograph. *Computer Graphics Forum*, 2013, 32(7): 101-110.

[28] Blinn J F. A generalization of algebraic surface drawing. *ACM Trans. Graph.*, 1982, 1(3): 235-256.

[29] O'Brien J F, Hodgins J K. Dynamic simulation of splashing fluids. In *Proc. the 1995 Computer Animation*, April 1995, pp.198-205.

[30] Murta A, Miller J. Modelling and rendering liquids in motion. In *Proc. the 7th International Conference in Central Europe on Computer Graphics, Visualization and Interactive Digital Media*, February 1999, pp.194-201.

[31] Fournier P, Habibi A, Poulin P. Simulating the flow of liquid droplets. In *Proc. the 1998 Graphics Interface Conference*, June 1998, pp.133-142.

[32] Kaneda K, Kagawa T, Yamashita H. Animation of water droplets on a glass plate. In *Proc. the 5th International Workshop on Computer Animation*, June 1993, pp.177-189.

[33] Kaneda K, Ikeda S, Yamashita H. Animation of water droplets moving down a surface. *The Journal of Visualization and Computer Animation*, 1999, 10(1): 15-26.

[34] Yu Y J, Jung H Y, Cho H G. A new water droplet model using metaball in the gravitational field. *Computers & Graphics*, 1999, 23(2): 213-222.

[35] Tong R, Kaneda K, Yamashita H. A volume-preserving approach for modeling and animating water flows generated by metaballs. *The Visual Computer*, 2002, 18(8): 469-480.

[36] Wolff L B. Using polarization to separate reflection components. In *Proc. the 1989 IEEE Computer Society Conference on Computer Vision and Pattern Recognition*, June 1989, pp.363-369.

[37] Lalonde J F, Narasimhan S G, Efros A A. What do the sun and the sky tell us about the camera? *International Journal of Computer Vision*, 2010, 88(1): 24-51.

[38] Hold-Geoffroy Y, Sunkavalli K, Hadap S, Gambaretto E, Lalonde J F. Deep outdoor illumination estimation. In *Proc. the 2017 IEEE International Conference on Computer Vision and Pattern Recognition*, July 2017, pp.2373-2382.

[39] Gardner M, Sunkavalli K, Yumer E, Shen X, Gambaretto E, Gagné C, Lalonde J F. Learning to predict indoor illumination from a single image. arXiv:1704.00090, 2017. https://arxiv.org/abs/1704.00090, June 2019.

[40] Georgoulis S, Rematas K, Ritschel T, Fritz M, Tuytelaars T, Gool L V. What is around the camera? In *Proc. the 2017 IEEE International Conference on Computer Vision*, October 2017, pp.5180-5188.

[41] Hold-Geoffroy Y, Sunkavalli K, Eisenmann J, Fisher M, Gambaretto E, Hadap S, Lalonde J. A perceptual measure for deep single image camera calibration. arXiv:1712.01259, 2017. https://arxiv.org/abs/1712.01259, June 2019.

[42] Xing G, Liu Y, Peng Q, Qin X. On-line illumination estimation of outdoor scenes based on area selection for augmented reality. In *Proc. the 12th International Conference on Computer-Aided Design and Computer Graphics*, September 2011, pp.439-442.

[43] Xing G, Liu Y, Qin X, Peng Q. A practical approach for real-time illumination estimation of outdoor videos. *Computers & Graphics*, 2012, 36(7): 857-865.

[44] Boivin S, Gagalowicz A. Image-based rendering of diffuse, specular and glossy surfaces from a single image. In *Proc. the 28th Annual Conference on Computer Graphics and Interactive Techniques*, August 2001, pp.107-116.

[45] Bousseau A, Paris S, Durand F. User-assisted intrinsic images. *ACM Trans. Graph.*, 2009, 28(5): Article No. 130.

[46] MacRobert T. Spherical Harmonics: An Elementary Treatise on Harmonic Functions with Applications (3rd rev. edition). Pergamon Press, 1967.

[47] Sillion F X, Arvo J R, Westin S H, Greenberg D P. A global illumination solution for general reflectance distributions. *ACM SIGGRAPH Comput. Graph.*, 1991, 25(4): 187-196.

[48] Ramamoorthi R, Hanrahan P. On the relationship between radiance and irradiance: Determining the illumination from images of a convex Lambertian object. *Journal of the Optical Society of America A, Optics, Image Science, and Vision*, 2001, 18(10): 2448-2459.

[49] Ramamoorthi R, Hanrahan P. An efficient representation for irradiance environment maps. In *Proc. the 28th Annual Conference on Computer Graphics and Interactive Techniques*, August 2001, pp.497-500.

[50] Ren H, Xu S, Wu S T. Effects of gravity on the shape of liquid droplets. *Optics Communications*, 2010, 283(17): 3255-3258.

[51] Dixit S, Pincus A, Guo B, Faris G. Droplet shape analysis and permeability studies in droplet lipid bilayers. *Langmuir: The ACS Journal of Surfaces and Colloids*, 2012, 28(19): 7442-7451.

[52] Sahin S, Bliznyuk O, Cordova R A, Schroën K. Microfluidic EDGE emulsification: The importance of interface interactions on droplet formation and pressure stability. *Scientific Reports*, 2016, 6: Article No. 26407.

[53] Li Z, Wang S, Yu J, Ma K L. Restoration of brick and stone relief from single rubbing images. *IEEE Transactions on Visualization and Computer Graphics*, 2012, 18(2): 177-187.

[54] Zhang T, Zhang L, Yu J. Computer generation of 3D inscriptions from 2D images of Chinese calligraphy. *Chinese Journal of Computers*, 2014, 37(11): 2380-2388. (in Chinese)

[55] Hamlyn D W. The Psychology of Perception: A Philosophical Examination of Gestalt Theory and Derivative Theories of Perception (1st edition). Routledge, 1957.

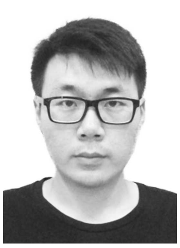

Mo-Han Zhang received his B.Sc. degree in software engineering from Sichuan University, Chengdu, in 2013. Currently, he is working toward his Ph.D. degree at the State Key Laboratory of CAD & CG, Zhejiang University, Hangzhou. His research interests include augmented reality, artistic augmentation, artificial intelligence and non-photorealistic rendering.

Jin-Hui Yu received his B.Sc. and M.Sc. degrees in electronics engineering from Harbin Shipbuilding Engineering Institute, Harbin Engineering University, Harbin, in 1982 and 1987, respectively. He received his Ph.D. degree in computer graphics from the University of Glasgow, Scotland, in 1999. He is a professor of computer science at the State Key Laboratory of CAD & CG, Zhejiang University, Hangzhou. He is also a guest professor at the Department of Computer Science, Harbin Finance University, Harbin. His research interests include image-based modeling, non-photorealistic rendering, computer animation, and computer graphics art.

Kang Zhang is a professor and director of Visual Computing Laboratory, Department of Computer Science at the University of Texas at Dallas (UT-Dallas), Richardson, U.S.A. He received his B.Eng. degree in computer engineering from University of Electronic Science and Technology of China, Chengdu, in 1982, his Ph.D. degree in computer science from University of Brighton, Brighton, UK, in 1990, and Executive MBA from the University of Texas at Dallas, Richardson, in 2011. Prior to joining UT-Dallas, he held academic positions in the UK, Australia, and China. Dr. Zhang's current research interests include visual languages, computational aesthetics, generative art, and software engineering, and he has published over 250 papers in these areas. He has authored and edited seven books. Dr. Zhang is an ACM Distinguished Speaker, and on the Editorial Boards of Journal of Big Data, The Visual Computer, Journal of Visual Languages and Computing, and International Journal of Software Engineering and Knowledge Engineering.

Jun-Song Zhang received his Ph.D. degree in computer science from State Key Laboratory of CAD & CG, Zhejiang University, Hangzhou, in 2008. He is currently a professor at National Engineering Research Center for E-Learning, Central China Normal University, Wuhan. His main research interests include computer graphics, computational aesthetics, Chinese information processing, and brain and cognitive science.

JOURNAL OF COMPUTER SCIENCE AND TECHNOLOGY

Volume 34, Number 6, November 2019

JOURNAL OF COMPUTER SCIENCE AND TECHNOLOGY

《计算机科学技术学报》

Volume 34 Number 6 2019 (Bimonthly, Started in 1986)

Indexed in: **SCIE, Ei, INSPEC, JST, AJ, MR, CA, DBLP**

Sponsored by: Institute of Computing Technology, CAS & China Computer Federation

Supervised by: Chinese Academy of Sciences

Undertaken by: Institute of Computing Technology, CAS

Published by: SCIENCE PRESS, BEIJING, CHINA

Printed by: Beijing Kexin Printing House

Distributed by:

China: All Local Post Offices

Other Countries: ORDER DEPT., SPRINGER, P.O. BOX 322, AH DORDRECHT, THE NETHERLAND

Available Online: www.springerlink.com

ISSN 1000-9000

国内统一连续出版物号: CN 11-2296/TP 国内邮发代号: 2-578 RMB ¥150.00